Synthetic Metals 191 (2014) 66–73

Contents lists available at ScienceDirect

Synthetic Metals

journal homepage: www.elsevier.com/locate/synmet

Synthesis of polypyrrole nano-fibers with hierarchical structure and its adsorption property of Acid Red G from aqueous solution

Jiangtao Feng[a], Jingjing Li[a], Wei Lv[a], Hao Xu[a], Honghui Yang[a,*], Wei Yan[b,*]

[a] Department of Environmental Science and Engineering, Xi'an Jiaotong University, Xi'an 710049, PR China
[b] State Key Laboratory of Multiphase Flow in Power Engineering, Xi'an Jiaotong University, Xi'an 710049, PR China

ARTICLE INFO

Article history:
Received 15 August 2013
Received in revised form 10 January 2014
Accepted 3 February 2014

Keywords:
Polypyrrole (PPy)
Hierarchical structure
Adsorption
Acid Red G

ABSTRACT

The polypyrrole nano-fibers with hierarchical structure were synthesized in α-CD/I_2 inclusion compound solution via chemical oxidation by using $FeCl_3$ as the oxidant. The formation of the hierarchical structured PPy was certified by Field Emission Scanning Electronic Microscope (SEM). Fourier transform infrared spectroscopy (FT-IR) results showed that the molecular structure of the prepared PPy backbone is same as the conventional PPy. From the results of X-ray fluorescence spectrometer (XRF) and X-ray diffraction (XRD) measurements, the α-CD/I_2-Fe^{2+} is as the soft-template during the synthesis process of PPy with hierarchical structure. Some I^- ions retained in the backbone of the prepared PPy were as the counter ion after rinse. PPy with hierarchical structure shows very good adsorption performance for the Acid Red G (azo dye). The adsorption equilibrium time was very short (within 30 min) and the maximum adsorption capacity (Q_{max}) was 121.95 mg/g, which is better than that of some other adsorbents reported in literatures. The hierarchical structured PPy that we prepared can be considered as a potential adsorbent for the removal of organic dyes from wastewater.

1. Introduction

After found as one of the conductive polymers, more and more interests are focus on polypyrrole (PPy) for its novel conductivity, environmental stability, bio-compatibility [1]. Furthermore, it has been successfully used in chemical and biological sensors [2–4], electromagnetic shielding [5,6], electrical switches [7], and so on. It is well known that the nano/micro-structure plays an important role in the performance of materials and further their applications. Although various morphologies of PPy, such as nanofibers [8,9], nanowires [10], micro/nanotubes [11,12], microsheets [13], microbowls and microcups [14] were synthesized by chemical and electrochemical methods. There are only a few publications about the hierarchical structured PPy. PPy with hierarchical structure can be achieved by using hierarchically organized architectures of bio-minerals [15] or other materials as the template [16,17].

Additionally, PPy can obtain the excellent conductive properties only when it is in the doped state. Actually, the doped PPy can contain several counter anions in its matrix [18–20]. The largest amount of the counter anions in the doped PPy is about 30% in mol ratio [21,22]. Moreover, the counter anions doped in PPy matrix can be organic or inorganic ions and can be exchanged by other ions [23]. Otherwise, Lu [24] et al. reported that the prepared hydro-sponge PPy consisting of nano-tubes had very good water absorption property and the water-storage of a saturated sample was about 65 g/g. In the view of this, conductive polymers (containing PPy) are considered as potential adsorbent materials to remove pollutions from water.

Recently, it attracts lots of interests in using PPy as the adsorbent to remove the pollutants from aqueous solutions. PPy doped with different organic or inorganic acid have selective adsorption behaviors of bovine serum albumin and lysozyme [25]. The composites formed from PPy and other polymers or semiconductor materials also had distinct adsorption capacities of organic and inorganic pollutions in water [26,27]. And the recent research found that polypyrrole-reduced graphene oxide composites synthesized by chemical or electrochemical route showed highly selective removal capacity of Hg^{2+} from water [28,29]. Furthermore, Fei et al. [30] declared that the morphologies obtained from different doping systems would have significant influence on the adsorption characteristics of the conductive polymers. For instance, the adsorption capacity of palyaniline micro/nanospheres was 20% higher than that of the palyaniline micro/nanofibers or sheets. These results indicated that the different dopants and the various

* Corresponding authors.
E-mail addresses: yanghonghui@mail.xjtu.edu.cn (H. Yang), yanwei@mail.xjtu.edu.cn (W. Yan).

http://dx.doi.org/10.1016/j.synthmet.2014.02.013
0379-6779/

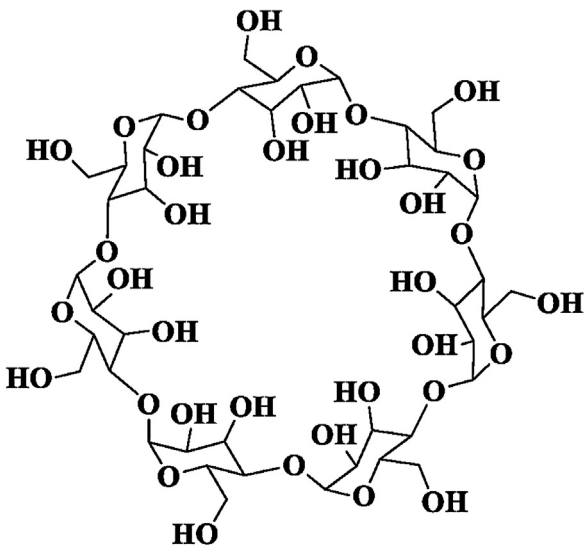

Fig. 1. Molecular structure of α-CD.

morphologies play the key role in the adsorption performance of conducting polymers.

Cyclodextrins, including α-CD, β-CD, γ-CD and their derivatives, have widely been used to prepare a variety of PPy or PANi with different morphologies and promote the physicochemical properties for their special molecular structure [31–34]. Therefore, alpha-cyclodextrin (α-CD) was employed to induce the formation of micro/nano-morphology PPy in this study. And PPy with hierarchical structure was synthesized in the solution containing α-CD and iodine via a chemical route by using $FeCl_3$ as the oxidant. The as-synthesized hierarchical structured PPy was used as the adsorbent to remove Acid Red G (ARG) from aqueous solution and demonstrated excellent adsorption.

2. Experimental

2.1. Materials

Pyrrole monomer (98%) was purchased from Qingquan Pharmaceutical & Chemical Ltd. (Zhejiang, China) and distilled under vacuum. The distilled pyrrole was stored in refrigeratory under the protection of nitrogen before used. Iodine (I_2) and potassium iodide (KI) were purchased from Sinopharm Chemical Reagent Co., Ltd. (Shanghai, China) as analytical reagent. Alpha-cyclodextrin (α-CD) was supplied by Liquan Chemical Industry Company (Shaanxi, China, biological grade) and its molecular structure is shown in Fig. 1. Ferric chloride hexahydrate ($FeCl_3{\cdot}6H_2O$, 98%, Beijing Chemicals) was used as the oxidant, ethanol (anhydrous, 99.8%, Sinopharm Chemical Reagent Co., Ltd., Shanghai, China) were used as-received. Acid Red G (5-acetamido-4-hydroxyl-3-(phenyliazenyl) naphthalene-2,7-disulfonic acid, ARG), Methyl Orange (4-[4-(dimethylamino)phenylazo]benzenesulfonic acid, MO) and Methylene Blue (3,7-bis(dimethylamino)phenazathionium chloride, MB) are commercial grade and recrystallized before used.

2.2. Preparation of the hierarchical structured PPy

The hierarchical structured PPy was synthesized by the soft-template method in α-CD/I_2 inclusion compound solution. The typical synthetic process is as follows. First, 10 mL KI·I_2 solution (12.7 g I_2 dissolved in 1000 mL 36 wt% KI solution) was added into the α-CD solution (0.5 mmol α-CD was dissolved in 30 mL deionized water) and stirred for 30 min at ambient temperature. The mixture solution was moved to a three-necked flask with mechanical stirring device and cooled to 5 °C. Then, pyrrole monomer (0.34 g, 5 mmol) was added to the mixture solution. After stirred for 30 min, $FeCl_3$ solution (1.0 mol/L, 12 mL) was dropwise added into the mixture. Then the polymerization process was continued another 24 h at 5 °C under static condition. Finally, the obtained black precipitate was washed with water and ethanol several times until the filtrate being colorless, followed by drying in vacuum oven at 50 °C for 24 h. The sample was named as H-PPy.

The synthesis route of conventional PPy sample (C-PPy) was similar with that of the H-PPy, except that no KI·I_2 and α-CD added.

2.3. Characterization

The morphologies were characterized by field emission scanning electron microscopy (FESEM, JSM-6700F, Japan). Transmission electron microscopy (TEM) was performed on a JEM model 2100 electron microscope. Fourier transform infrared spectra (FT-IR) of samples were measured by the KBr pellet method on a BRUKER TENSOR 37 FT-IR spectrophotometer in the range of 4000–400 cm^{-1}. The elements of the samples were characterized in the X-ray fluorescence spectrometer (XRF, S4 PIONEER, Bruker, Germany). X-ray diffraction (XRD) patterns of the samples were obtained with an X'Pert PRO MRD Diffractometer using Cu-Kα radiation. The BET surface area (S_{BET}), total pore volume (V) and average pore radius (R) were measured at 77 K using Builder SSA-4200 (Beijing, China).

2.4. Adsorption experiments

All adsorption experiments were carried out in the dark condition at ambient temperature. The suspension containing 200 mg/L of Acid Red G (ARG) solution and 2 g/L of adsorbent was stirred for 1 h. Then the suspension was centrifuged at 4000 rpm for 5 min. The supernatant was analyzed by the UV–vis spectrophotometer (Agilent 8453, American). The absorbance value of ARG was read at the wavelength of 503 nm. The adsorptions of MB and MO onto H-PPy were carried out as same as that of ARG accept for the different wavelength (665 nm for MB and 465 nm for MO).

The effect of the dose of adsorbent on the ARG adsorption was studied by adding different mass (0.08–4 g/L) of adsorbent into 200 mg/L ARG solution. The influence of pH value on the ARG (200 mg/L) removal was studied in the pH range of 2–12. The pH was adjusted by NaOH or HNO_3 solution.

The adsorption rate R (%) and the amount of dye molecules adsorbed on the adsorbents Q_t (mg/g) at certain time t were calculated from Eqs. (1) and (2), respectively:

$$R(\%) = \frac{C_0 - C_t}{C_0} \times 100 \quad (1)$$

$$Q_t(\mathrm{mg/g}) = \frac{C_0 - C_t}{M \times V} \quad (2)$$

where C_0 is the initial concentration (mg/L) of ARG, C_t is the residual concentration at time t (mg/L), V is the solution volume (L), and M is the adsorbent mass (g).

Adsorption isotherms of ARG on H-PPy and C-PPy at 25 °C were obtained by mixing different concentrations (50–700 mg/L) of ARG solutions with 2 g/L of adsorbent. Langmuir and Freundlich isotherms are described in linear forms according to Eqs. (3) and (4), respectively:

$$\frac{C_{eq}}{Q_{eq}}(\mathrm{g/L}) = \frac{1}{Q_{\max}K_L} + \frac{C_{eq}}{Q_{\max}} \quad (3)$$

$$\log Q_{eq}(\mathrm{mg/g}) = \log K_F + n\log C_{eq} \quad (4)$$

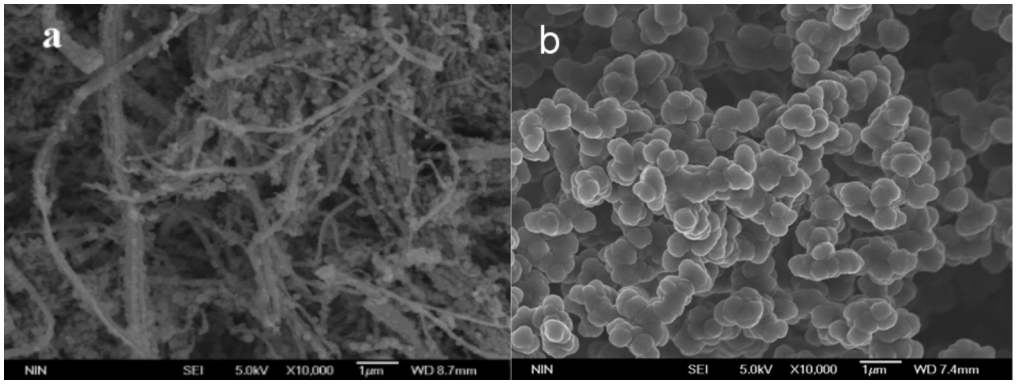

Fig. 2. Morphologies of H-PPy (a) and C-PPy (b).

where C_{eq} (mg/L) is ARG equilibrium concentration; Q_{max} (mg/g) is the maximum adsorption capacity; K_L (L/mg) is a constant that related to the heat of adsorption; K_F (mg/g) represents the adsorption capacity when C_{eq} equals 1; n represents the dependence degree of adsorption on equilibrium concentration.

For thermomechanical analysis, the adsorption isotherm experiments were further repeated in 15 and 35 °C, respectively.

3. Results and discussion

3.1. Characterizations of the samples

The morphology of the H-PPy prepared in the KI·I_2 and α-CD system is the same as the sprout in the branch which is often called hierarchical structure in chemistry [35,36]. The diameter of the branches in the hierarchical structure is under 100 nm while the size of the sprout is in the range of 100–200 nm (Fig. 2a). However, the morphology of C-PPy prepared by conventional method is the traditional cauliflower, as shown in Fig. 2b [37]. This suggested that the KI·I_2 and α-cyclodextrin system was the critical factor for the formation of H-PPy. In FT-IR spectra (Fig. 3), it is considered that the C=C ring stretching band of pyrrole occurred at 1534 cm^{-1} is for quinonoid structure of PPy. The band at 1471 cm^{-1} is attributed to C—N stretching vibration in pyrrole ring. Additionally, peaks at 1296, 1168 and 1032 cm^{-1} are ascribed to =C—H vibration on plane, and peak at 910 cm^{-1} is for =C—H out-of-plane vibration [38–41]. This indicated that the backbone of the PPy prepared in the KI·I_2 and α-CD system is the same as that of PPy prepared by conventional route.

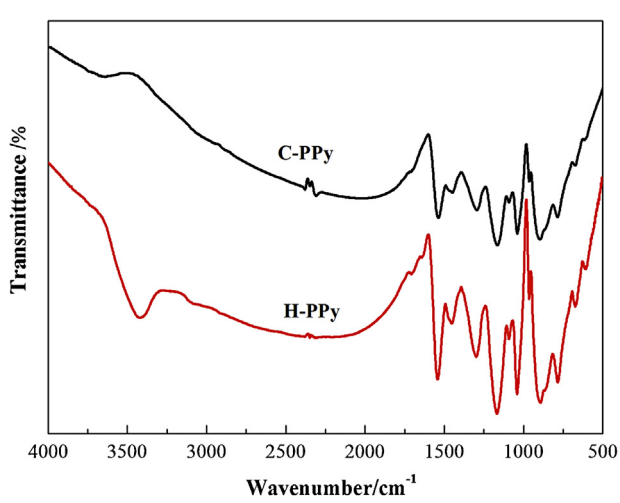

Fig. 3. FT-IR spectra of H-PPy and C-PPy.

3.2. Formation mechanism of the hierarchical structure PPy

In order to understand the formation mechanism of H-PPy, the SEM images of α-CD/I_2-Fe^{3+} and α-CD/I_2-Fe^{2+} complexes are shown in Fig. 4, while the TEM images of α-CD/I_2-Fe^{3+} and α-CD/I_2-Fe^{2+} complexes and hierarchical PPy are displayed in Fig. 5. The morphology of α-CD/I_2-Fe^{3+} shows the large number of rod-like morphology and the TEM image also testifies this structure (Fig. 5a), which is very different from the morphology of H-PPy. It is obviously noticed that the α-CD/I_2-Fe^{2+} complex has the rigid fibrous structure and the TEM image also displays the same good configuration (Fig. 5b), which was very similar with H-PPy. Meanwhile, the TEM image of H-PPy shows that many particles buildup the Hierarchical structure (Fig. 5c). Some publications reported that the complexes were formed between Fe^{m+} and the inclusion compounds of cyclodextrins [13,32]. So it is considered that H-PPy might be prepared initially with the structure of α-CD/I_2-Fe^{2+} complex and then grew up to the final hierarchical structure along this trend. To improve this process, the XRF characterizations of the samples, including the α-CD/I_2 inclusion compound, α-CD/I_2-Fe^{2+}complex, H-PPy before and after rinse, were also performed. XRF results (Table 1) show that the changes of the main elements in the PPy matrix resulted from the synthesis process. As the oxidant (Fe^{3+}), the content of Fe increases firstly and then decreases. The content of Fe in α-CD/I_2 inclusion compound is almost zero, while it is 1.24% in α-CD/I_2-Fe^{2+}. After rinse, the content of Fe in H-PPy is much equal to the value of that in α-CD/I_2 inclusion compound. The content of iodine in these samples experiences the same trend with Fe. The difference is the content of iodine was higher in all these samples and is greater than zero in hierarchical structure PPy after rinse (19.1%). While the content of K (from KI·I_2 solution) decreases from 5.92% in α-CD/I_2 inclusion compound to nearly 0 in the hierarchical structured PPy after rinse. In contrast, the content of Cl increases from nearly 0 in α-CD/I_2 inclusion compound to 19.7% in the hierarchical structure PPy after rinse. From these evidences, the contents of ions in PPy matrix from synthesis process decrease after the PPy sample rinsed except Cl. In many reports, Cl^- is as the counter ion in doped PPy matrix [42]. The content of iodine decrease after rinse while that

Table 1
the results of XRF for samples.

Samples	Amounts of elements (wt%)			
	Fe	Cl	I	K
α-CD/I_2 inclusion compound	0.046	0.103	37.1	5.92
α-CD/I_2-Fe^{2+}complex	1.24	0.305	46.5	0.371
H-PPy before rinse	0.0789	6.42	33.8	0.0411
H-PPy after rinse	0.0416	19.7	19.1	0.0389

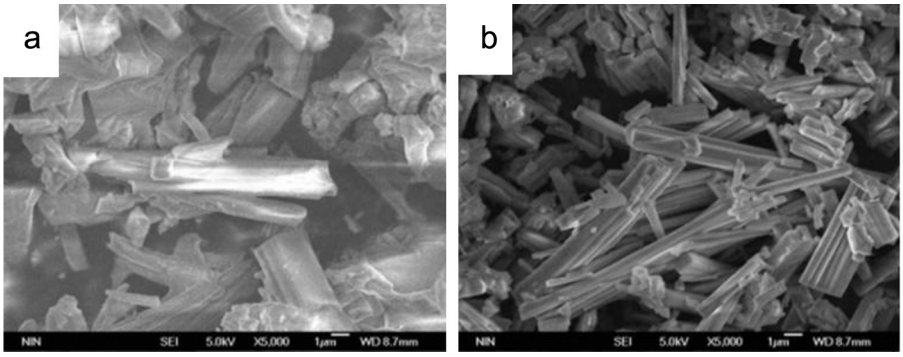

Fig. 4. SEM images of (a) α-CD/I_2-Fe^{3+} and (b) α-CD/I_2-Fe^{2+}.

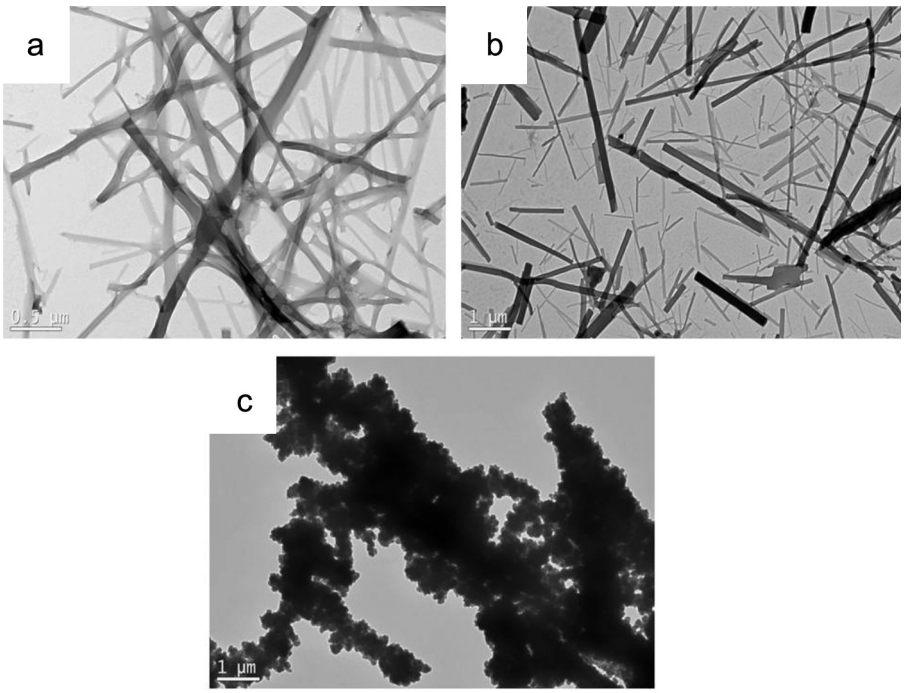

Fig. 5. TEM images of (a) α-CD/I_2-Fe^{3+}, (b) α-CD/I_2-Fe^{2+} and (c) H-PPy.

of Cl increase demonstrates that Cl^- may be more firmly combined with PPy backbone than I^- as the counter ion in doped PPy matrix. The decrease of I and Fe indicates that H-PPy contains a certain amount of α-CD/I_2-Fe^{2+}, which can be rinsed from the synthesized PPy and some of I^- was still stay in PPy matrix as the counter ion. All of these evidences indicate that the α-CD/I_2-Fe^{2+} complex play the initial model during the synthetic process of H-PPy. Meanwhile, I^- is not only as the part of the soft-model in the synthesis process of H-PPy, but also as the counter ion in the as-prepared PPy matrix. This is also proved by XRD patterns (Fig. 6). In XRD patterns, α-CD/I_2 inclusion compound shows good crystal properties for its excellent crystal diffraction peak. The α-CD/I_2-Fe^{2+} complex exhibits a distinct diffraction peak at nearly $2\theta = 18°$, which is also the main peak in the diffraction of α-CD/I_2 inclusion compound. However, there is a wide peak in the patterns of H-PPy before and after rinse, which demonstrates that the as-prepared PPy are amorphous. Meanwhile, there is still one small sharp peak in the XRD pattern of H-PPy before and after rinse respectively, corresponding to the same position of 2θ *in* the XRD patterns of α-CD/I_2-Fe^{2+}, which may indicate that some of the α-CD/I_2-Fe^{2+} complex could not be rinsed from the as-prepared PPy matrix. The phenomena are very similar to the literature [43]. So the formation

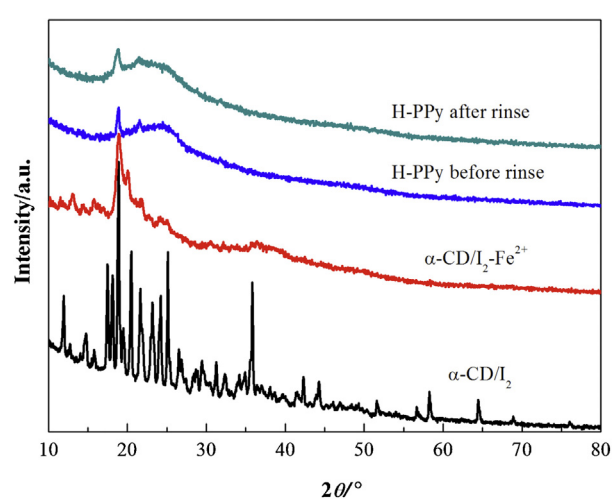

Fig. 6. XRD patterns of samples.

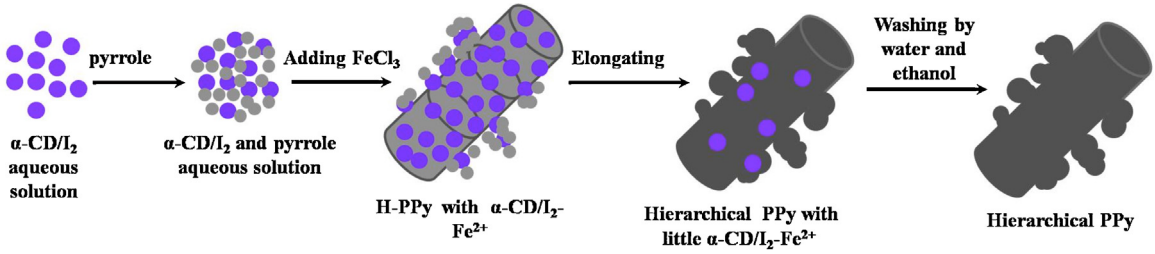

Fig. 7. Illustration of the formation mechanism of the hierarchical PPy.

mechanism of the H-PPy is supposed as follow: firstly, α-CD and I_2 formed inclusion compounds in aqueous solution under stirring. And the intensive mixture of α-CD/I_2 inclusion compounds and small pyrrole droplets were obtained after adding pyrrole with vigorous stirring. The PPy with incompact rod-like structure was synthesized by the accession of $FeCl_3$ solution. With the increase of the reaction, more and more Fe^{3+} was reduced to Fe^{2+}, which induces the formation of more α-CD/I_2-Fe^{2+} complexes. Moreover, α-CD/I_2-Fe^{2+} complexes were easily to emerge fibrous structure. The rod-like PPy formed in the initial process could elongate along the direction of α-CD/I_2-Fe^{2+} complexes to establish fiber morphology. However, some of the rod-like PPy were not ready to grow along the α-CD/I_2-Fe^{2+} complex fiber, and they were only able to elongate on the surface of the fiber. Therefore, the PPy with hierarchical structure was obtained by this process (Fig. 7). Furthermore, the α-CD/I_2-Fe^{2+} complexes can break away from the formed PPy in all process, especially the rinse process, which was well proved by the data of XRF. But few α-CD/I_2-Fe^{2+} complexes coated in the initial PPy rod were hard to be eluted from PPy, which resulted in the detection of ferrum can be detected by XRF and XRD.

3.3. Adsorption properties of as-prepared PPy

PPy has been used as the potential materials to remove some organic or inorganic substances from water in recent years [26,28]. In order to study the adsorption performance of the samples, we characterized the specific surface area of the samples which is considered to have great relevance with adsorption properties. Fig. 8 shows the nitrogen adsorption–desorption isotherms of C-PPy and H-PPy. Both isotherms of C-PPy and H-PPy are typical of mesoporous adsorbent. The difference is the obvious hysteresis loop in the isotherm of C-PPy in desorption phase as the relative pressure is above 0.4. However, this hysteresis loop is hardly noticed in the isotherm of H-PPy and the relative pressure range of the hysteresis loop is comparatively concentrated, which indicates that the pore size distribution of H-PPy is more uniform than that of C-PPy.

Table 2
The BET data of the samples.

Samples	S_{BET} (m^2/g)	V (cm^3/g)	R (nm)
C-PPy	13.69	0.098	14.37
H-PPy	42.94	0.25	11.59

The BET surface area (S_{BET}), total pore volume (V) and average pore radius (R) of H-PPy and C-PPy particles were measured and listed in Table 2. The N_2 isotherms at 77 K showed a clearly increase of the BET surface area of H-PPy (S_{BET} = 42.94 m^2/g) compared with C-PPy (S_{BET} = 13.69 m^2/g), which increased more than 3 times. At the same time, the pore volume of H-PPy (V = 0.25 cm^3/g) is also higher than that of C-PPy (V = 0.098 cm^3/g), which is more than twice as large as the pore volume of the conventional particle PPy. The larger BET surface area and pore volume would be advantageous for adsorption of H-PPy.

Fig. 9 shows that the adsorption capacity of H-PPy and C-PPy for ARG is varied with the adsorption time. It is clearly noted that the adsorption of ARG on H-PPy and C-PPy can reach equilibrium in 60 min. It also shows that the equilibrium adsorption capacity of H-PPy is twice higher than that of C-PPy particles.

Fig. 10 shows the linear forms for the adsorption isotherm, and the related parameters are calculated and listed in Table 3. The results indicate that the adsorption behavior of ARG on H-PPy and C-PPy can be described by the Langmuir model, for its correlation coefficient (R^2 = 0.9990) is better than that of Freundlich model (not be shown here). The maximum adsorption amounts of ARG on H-PPy and C-PPy particles are 121.95 mg/g and 53.68 mg/g, respectively. This is very close to the experimental data, 115.88 mg/g and 50.61 mg/g for H-PPy and C-PPy particles, respectively. Meanwhile, the adsorption capacity of ARG on H-PPy may be no less than that of some other adsorbents. The adsorption capacities of some adsorbents for Acid Red dyes are listed in Table 4. It can be seen that the adsorption capacity of H-PPy is satisfied, compared with some other adsorbents already reported in literatures. Moreover, the

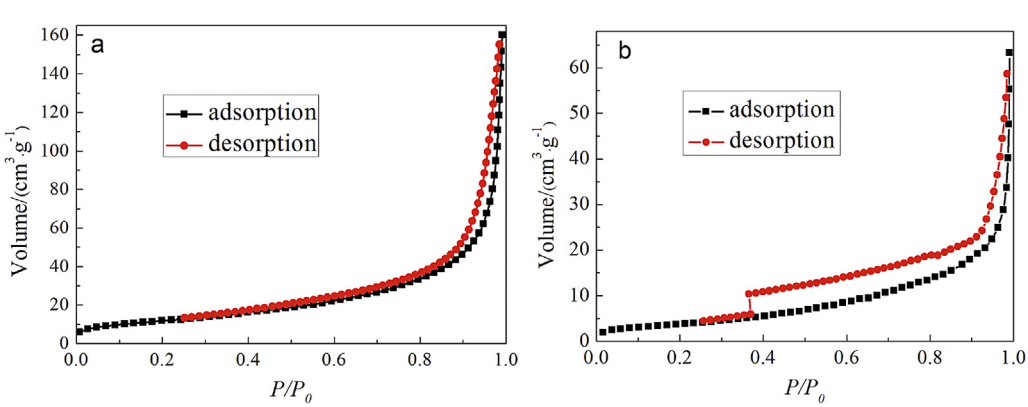

Fig. 8. Adsorption–desorption isotherms of N_2 at 77 K of H-PPy (a) and C-PPy (b).

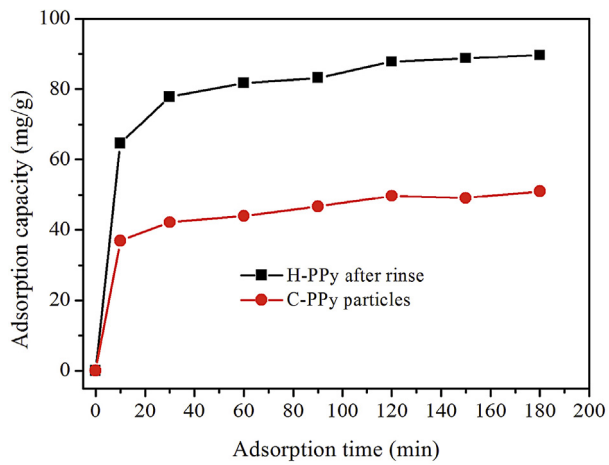

Fig. 9. Adsorption capacity of H-PPy and C-PPy.

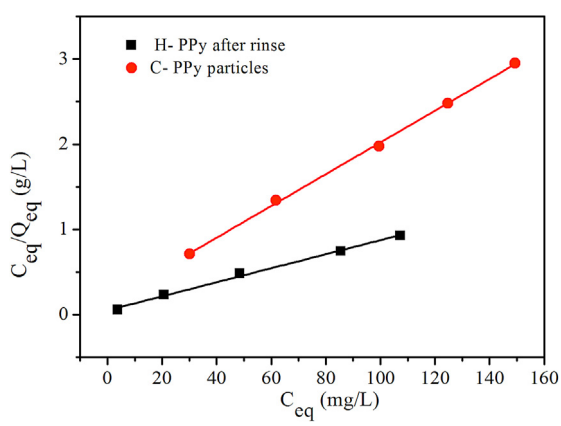

Fig. 10. Langmuir isotherm of ARG on PPy: the dots are the original data and the liner forms are Langmuir isotherm model.

equilibrium adsorption time of H-PPy in this paper is equal or less than that of other adsorbents in the list. These results indicate that the as-prepared hierarchical structured PPy as the adsorbent has more efficient adsorption capacity.

It is believed that the pH value can affect the interaction between PPy backbone and the dopants. The dopants will be break away from the PPy backbone in alkaline conditions [49]. Many researchers considered that the adsorption property of the conducting polymers is due to their doping effect. In other words, the

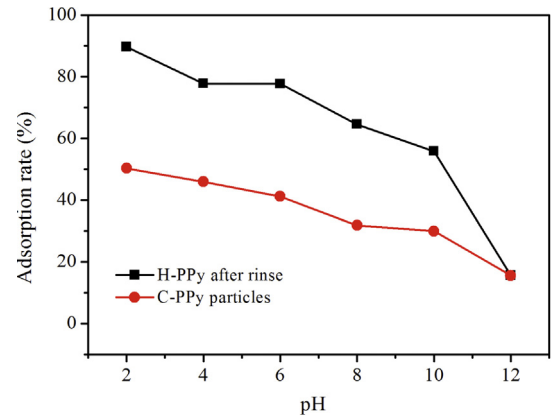

Fig. 11. Effects of pH value on the adsorption capacities of as-prepared PPy.

adsorbates are as the counter ions in the backbone of the conductive polymers [50]. Therefore, the adsorption capacity of the conductive polymers will decrease with increasing the pH value of the solution for de-doping of the counter ions in polymer matrix. The effect of pH value on the adsorption capacity of H-PPy and C-PPy particle are tested, as shown in Fig. 11. It can be seen that the adsorption capacity of each PPy sample descends with the increase of the solution pH value. When the pH value is larger than 10, the adsorption capacities of H-PPy and C-PPy have a sharp decrease with the increase of the pH value. It descends to a low level which is same as that of the conventional PPy particle when pH = 12. Part of adsorption performances for both hierarchical structured PPy and conventional PPy particle have been retained when pH = 12.

The thermodynamic parameters, such as changes of standard Gibbs free energy (ΔG°), entropy (ΔS°) and enthalpy (ΔH°), can be used to represent the trend of chemical or physical process. The parameters for adsorption of ARG by as-prepared PPy samples were determined by following equations:

$$\ln K_L = \frac{\Delta S^\circ}{R} + \frac{-\Delta H^\circ}{RT} \quad (5)$$

$$\Delta G^\circ = -RT \ln K_L \quad (6)$$

where R (=8.314 J/(mol K)) is the gas constant and T (K) is the temperature. K_L (L/mg) is Langmuir adsorption constant. ΔH° and ΔS° can be calculated from the slope and intercept of vant Hoff plots of $\ln K_L$ versus $1/T$. The parameters were listed in Table 5. The positive value of ΔH° indicated that the process was endothermic in nature, while the positive of ΔS° declared that an increase in disorder at the solid-solution interface during the adsorption of dye.

Table 3
Parameters of Langmuir and Freundlich adsorption isotherm models at 25 °C.

Adsorbent	Langmuir model			Freundlich model		
	Q_{max} (mg/g)	K_L (L/mg)	R^2	K_F (mg/g)	n	R^2
H-PPy	121.95	0.1630	0.9955	52.40	0.1724	0.9953
C-PPy	53.76	0.1176	0.9990	28.55	0.1174	0.9462

Table 4
Comparison of the adsorption capacity of H-PPy with other adsorbents for azo dyes.

Adsorbents	Azo dyes	Q_{max} (mg/g)	Equilibrium time (min)	Reference
H-PPy	Acid Red G	121.95	30	This work
C-PPy particle	Acid Red G	53.68	30	This work
Activated carbon	Acid Red 97	52.08	30	[44]
$CuFe_2O_4$ powder	Acid Red B	86.8	30	[45]
Montmori-llonite	Acid Red G	171.53	60	[46]
Calcined-alunite	Acid Red 57	80.02	120	[47]
Polyaniline nanotubes	Methylene Blue	4.8	120	[48]

Table 5
Thermodynamic and Langmuir parameters for ARG adsorption on H-PPy at different temperatures.

T (K)	Q_{max} (mg/g)	K_L (L/mg)	ΔG° (kJ/mol)	ΔS° (J/mol K)	ΔH° (kJ/mol)
288	97.09	0.1570	−18.99		
298	121.95	0.1630	−19.64	81.19	6.93
308	135.14	0.1897	−20.30		

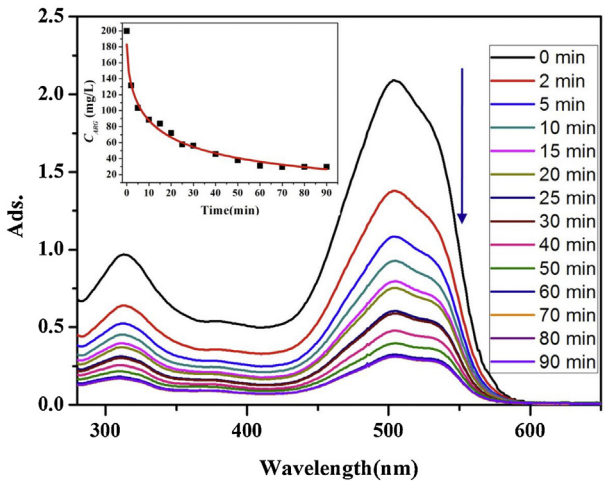

Fig. 12. Change of ARG UV–vis spectra in real-time (insert is the change of ARG concentration in real-time).

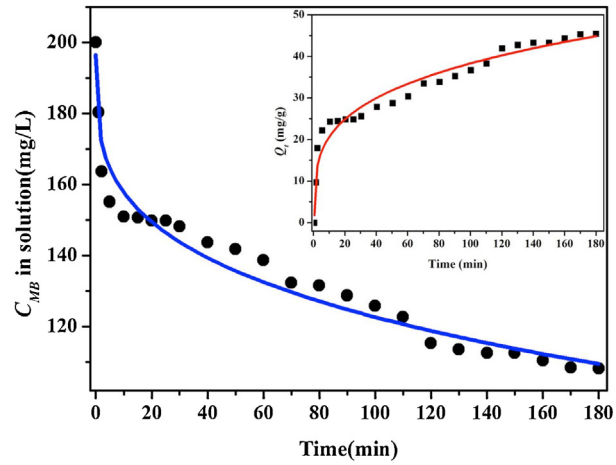

Fig. 14. Change of MB concentration in solution and the adsorption quantity of MB in H-PPy (insert) with adsorption time.

The ΔG° is negative at different temperatures using in this study, which determined that the adsorption process was spontaneous.

3.4. Adsorption mechanism

The adsorption of dye molecules on adsorbents may be dominated by physical, chemical and the combination of the two at the surface. Many studies show that the adsorption of dyes on PPy can proceed by electrostatic interaction and hydrogen bonding but the electrostatic interaction plays the major role [25,26,51]. Moreover, the electrostatic interaction mainly occurs between the dye and the radical N atoms in the backbone of PPy and the hydrogen bonding usually combines the hydrogen binding in inactive N of PPy [52]. These interactions are both the short-range force, which is the reason that the adsorption behavior of dye on PPy complies with Langmuir model that is a monolayer adsorption model. It can also explain the high rate in the initial stage of adsorption, and it decrease clearly along with the adsorption time. It is also confirmed by the change of UV–vis spectra during the adsorption of Acid Red G on H-PPy in real-time (Fig. 12). The change of MB and MO concentrations in solution during the adsorption are the same as well except for the little adsorption capacity (Figs. 13 and 14). So, the major interaction for the adsorption of ARG, MO and MB on H-PPy is electrostatic interaction and the hydrogen bonding plays the secondary action.

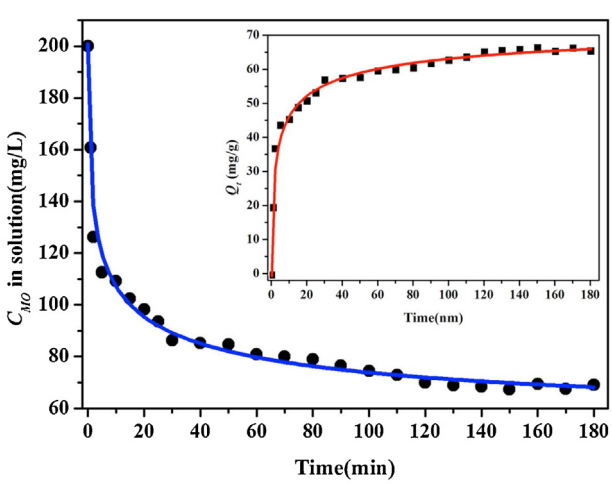

Fig. 13. Change of MO concentration in solution and the adsorption quantity of MO in H-PPy (insert) with adsorption time.

4. Conclusions

The polypyrrole nano-fibers with hierarchical structure were synthesized. The diameter of the fiber is 100 nm and the length of the fiber is over 20 μm. The size of the sprout in the fibers is in the range of 100–200 nm. It is considered that the hierarchical structured PPy grows up with α-CD/I_2-Fe^{2+} complex and some of I^- ions stay in the backbone of the as-prepared PPy as the counter ions although Cl^- is more firmly combined with PPy backbone than I^- in doped PPy matrix. The H-PPy shows a better adsorption property to removal ARG in aqueous solution than the C-PPy does. It can reach the maximum adsorption value of 121.95 mg/g in 30 min, which is better than that of some other adsorbents. The major interaction for the adsorption of ARG on H-PPy is electrostatic interaction and the hydrogen bonding plays the secondary action, which is also utilized to other organic dyes, such as MO and MB. The H-PPy can be considered as a potential adsorbent for the removal of organic dyes from wastewater.

Acknowledgments

The authors gratefully acknowledge the financial supports from the National Natural Science Foundation of China (Grant no. 21307098), China Postdoctoral Science Foundation (2013M532053) and the Fundamental Research Funds for the Central Universities of China.

References

[1] N. Ballav, A. Maity, S.B. Mishra, High efficient removal of chromium (VI) using glycine doped polypyrrole adsorbent from aqueous solution, Chem. Eng. J. 198 (2012) 536–546.
[2] O.S. Kwon, S.J. Park, H. Yoon, J. Jang, Highly sensitive and selective chemiresistive sensors based on multidimensional polypyrrole nanotubes, Chem. Commun. 48 (2012) 10526–10528.
[3] M. Braiek, H. Barhoumi, A. Maaref, N. Jaffrezic-Renault, Elaboration and characterization of pH sensor based on polypyrrole nanowires, Sensor Lett. 9 (2011) 2154–2157.
[4] J. Rick, T.C. Chou, Ampermetric protein sensor – fabricated as a polypyrrole, poly-aminophenylboronic acid bilayer, Biosens. Bioelectron. 22 (2006) 329–335.
[5] E. Hakansson, A. Amiet, S. Nahavandi, A. Kaynak, Electromagnetic interference shielding and radiation absorption in thin polypyrrole films, Eur. Polym. J. 43 (2007) 205–213.
[6] C.Y. Huang, J.Y. Wu, K.Y. Tsao, C.L. Lin, C.P. Chang, C.S. Tsai, Y.H. Chen, J.T. Yeh, K.N. Chen, The manufacture and investigation of multi-walled carbon nanotube/polypyrrole/EVA nano-polymeric composites for electromagnetic interference shielding, Thin Solid Films 519 (2011) 4765–4773.
[7] L. Fang, T.Y. Dai, Y. Lu, Electromagnetic composite films based on polypyrrole hydro-sponge and Fe_3O_4 ferrofluid, Synth. Met. 159 (2009) 2101–2107.
[8] S. Sahoo, S. Dhibar, C.K. Das, Facile synthesis of polypyrrole nanofiber and its enhanced electrochemical performances in different electrolytes, Express Polym. Lett 6 (2012) 965–974.
[9] J.F. Zang, C.M. Li, S.J. Bao, X.Q. Cui, Q.L. Bao, C.Q. Sun, Template-free electrochemical synthesis of superhydrophilic polypyrrole nanofiber network, Macromolecules 41 (2008) 7053–7057.
[10] L. Xia, B.G. Quan, Z.X. Wei, Patterned growth of vertically aligned polypyrrole nanowire arrays, Macromol. Rapid Commun. 32 (2011) 1998–2002.
[11] B. Schulz, I. Orgzall, I. Díez, B. Dietzel, K. Tauer, Template mediated formation of shaped polypyrrole particles, Colloids. Surf. A: Physicochem. Eng. Aspects 354 (2010) 368–376.
[12] J. Han, W. Yan, Y.B. Xu, Synthesis of long polypyrrole micro/nanotubules with rectangular sections, Chem. Lett. 35 (2006) 306–307.
[13] J.T. Feng, W. Yan, J.W. Zhu, Synthesis of novel hexagonal micro-sheet polypyrrole and micro-sheet polypyrrole with grooves in the presence of α-cyclodextrin-Acid Red G inclusion compounds, Synth. Met. 60 (2010) 939–945.
[14] L.T. Qu, G.Q. Shi, F.E. Chen, J.X. Zhang, Electrochemical growth of polypyrrole microcontainers, Macromolecules 36 (2003) 1063–1067.
[15] Y. Oaki, M. Kijima, H. Imai, Synthesis and morphogenesis of organic polymer materials with hierarchical structures in biominerals, J. Am. Chem. Soc. 133 (2011) 8594–8599.
[16] X.J. Lu, F. Zhang, H. Dou, C.Z. Yuan, S.D. Yang, L. Hao, L.F. Shen, L.J. Zhang, X.G. Zhang, Preparation and electrochemical capacitance of hierarchical graphene/polypyrrole/carbon nanotube ternary composites, Electrochim. Acta 69 (2012) 160–166.
[17] Y.Q. Han, X.T. Qing, S.J. Ye, Y. Lu, Conducting polypyrrole with nanoscale hierarchical structure, Synth. Met. 160 (2010) 1159–1166.
[18] M. Yamaura, K. Sato, T. Hagiwara, Effect of counter-anion exchange on electrical-conductivity of polypyrrole films, Synth. Met. 39 (1990) 43–60.
[19] N.V. Blinova, J. Stejskal, M. Trchova, J. Prokes, M. Omastova, Polyaniline and polypyrrole: a comparative study of the preparation, Eur. Polym. J. 43 (2007) 2331–2341.
[20] M. Yamaura, K. Sato, T. Hagiwara, K. Iwata, Memory effect of electrical conductivity upon the counteranion exchange of polypyrrole films, Synth. Met. 48 (1992) 337–354.
[21] K. Idla, A. Talo, H.E.M. Niemi, O. Forsen, S. Ylasaari, An XPS and AFM study of polypyrrole coating on mild steel, Surf. Interface Anal. 25 (1997) 837–854.
[22] D.Y. Kim, J.Y. Lee, C.Y. Kim, E.T. Kang, K.L. Tan, Difference in doping behavior between polypyrrole films and powders, Synth. Met. 72 (1995) 243–248.
[23] A. Michalska, K. Maksymiuk, Counter-ion influence on polypyrrole potentiometric pH sensitivity, Microchim. Acta 143 (2003) 163–175.
[24] T.Y. Dai, Y. Lu, Polypyrrole hydro-sponges built up from mesoscopic scales, J. Mater. Chem. 17 (2007) 4797–4802.
[25] X. Zhang, R.B. Bai, Y.W. Tong, Selective adsorption behaviors of proteins on polypyrrole-based adsorbents, Sep. Purif. Technol 52 (2006) 161–169.
[26] X. Zhang, R.B. Bai, Adsorption behavior of humic acid onto polypyrrole-coated nylon 6,6 granules, J. Mater. Chem. 12 (2002) 2733–2739.
[27] C.W. Lim, K. Song, S.H. Kim, Synthesis of PPy/silica nanocomposites with cratered surfaces and their application in heavy metal extraction, J. Ind. Eng. Chem. 18 (2012) 24–28.
[28] V. Chandra, K.S. Kim, Highly selective adsorption of Hg^{2+} by a polypyrrole-reduced graphene oxide composite, Chem. Commun. 47 (2011) 3942–3944.
[29] Z.Q. Zhao, X. Chen, Q. Yang, J.H. Liu, X.J. Huang, Selective adsorption toward toxic metal ions results in selective response: electrochemical studies on a polupyrrole/reduced graphene oxide nanocomposite, Chem. Commun. 48 (2012) 2180–2182.
[30] X. Guo, G.T. Fei, H. Su, L.D. Zhang, Synthesis of polyaniline micro/nanospheres by a copper (II)-catalyzed self-assembly method with superior adsorption capacity of organic dye from aqueous solution, J. Mater. Chem. 21 (2011) 8618–8625.
[31] S.M. Shang, W. Zeng, X.M. Tao, Fabrication of conducting polypyrrole/beta-cyclodextrin nano-and microspheres using molecular templates, RSC Adv. 2 (2012) 4675–4682.
[32] X.Q. Hu, Y. Lu, J.H. Liu, Synthesis of polypyrrole microtubes with actinomorphic morphology in the presence of a beta-cyclodextrin derivative-methyl orange inclusion complex, Macromol. Rapid Commun. 25 (2004) 1117–1120.
[33] U. Tamer, C. Kanbes, H. Torul, N. Ertas, Preparation, characterization and electrical properties of polyaniline nanofibers containing sulfonated cyclodextrin group, React. Funct. Polym. 71 (2011) 933–937.
[34] A. Prasannan, L.B.T. Tram, P.D. Hong, N. Somanathan, I. Shown, T. Imae, Synthesis and characterization of "Hairy Urchin"-like polyaniline by using beta-cyclodextrin as a template, Langmuir 27 (2011) 766–773.
[35] D.J. Lee, H.M. Kim, Y.S. Song, J.R. Youn, Water droplet bouncing and superhydrophobicity induced by multiscale hierarchical nanostructures, ACS Nano 6 (2012) 7656–7664.
[36] W.A. Lopes, H.M. Jaeger, Hierarchical self-assembly of metal nanostructures on diblock copolymer scaffolds, Nature 414 (2001) 735–738.
[37] T.C. Wen, S.L. Hung, M. Diger, Effect of polypyrrole on the morphology and ionic conductivity of TPU electrolyte containing $LiClO_4$, Synth. Met. 118 (2001) 11–18.
[38] H.N.M.E. Mahmud, A. Kassim, Z. Zainal, W.M.M. Yunus, Fourier transform infrared study of polypyrrole-poly(vinyl alcohol) conducting polymer composite films: evidence of film formation and characterization, J. Appl. Polym. Sci. 100 (2006) 4107–4113.
[39] X.M. Yang, Y. Lu, Hollow nanometer-sized polypyrrole capsules with controllable shell thickness synthesized in the presence of chitosan, Polymer 46 (2005) 5324–5328.
[40] J. Liu, M.X. Wan, Studies on formation mechanism of polypyrrole microtubule synthesized by template-free method, J. Polym. Sci. A: Polym. Chem. 39 (2001) 997–1004.
[41] J.Y. Jin, T. Ando, N. Teramae, H. Haraguchi, Characterization of electropolymerized polypyrrole films by FT-IR reflection absorption-spectroscopy, Bunseki Kagaku 40 (1991) 799–804.
[42] W.M. Aylward, P.G. Pickup, Anion and cation transport in composite films of polypyrrole with a sulphonated silica (ormosil) hydrogel, Electrochim. Acta 52 (2007) 6275–6281.
[43] W. Yan, J. Han, Synthesis and formation mechanism study of rectangular-sectioned polypyrrole micro/nanotubules, Polymer 48 (2007) 6782–6790.
[44] V. Gomez, M.S. Larrechi, M.P. Callao, Kinetic and adsorption study of acid dye removal using activated carbon, Chemosphere 69 (2007) 1151–1158.
[45] R.C. Wu, H.H. Qu, H. He, Y.B. Yu, Removal of azo-dye Acid Red B (ARB) by adsorption and catalytic combustion using magnetic $CuFe_2O_4$ powder, Appl. Catal. B: Environ. 48 (2004) 49–56.
[46] D.S. Tong, C.H. Zhou, Y. Lan, H.Y. Yu, G.F. Zhang, W.H. Yu, Adsorption of Acid Red G dye on octadecyl trimethylammonium montmorillonite, Appl. Clay Sci. 50 (2010) 427–431.
[47] S. Tunali, A.S. Ozcan, A. Ozcan, T. Gedikbey, Kinetics and equilibrium studies for the adsorption of Acid Red 57 from aqueous solutions onto calcined-alunite, J. Hazard. Mater. 135 (2006) 141–148.
[48] M.M. Ayad, A. Abu El-Nasr, Adsorption of cationic dye (methylene blue) from water using polyaniline nanotubes base, J. Phys. Chem. C 114 (2010) 14377–14383.
[49] M.M. Castillo-Ortega, I. Santos-Sauceda, J.C. Encinas, D.E. Rodriguez-Felix, T. Castillo-Castro, F. Rodriguez-Felix, J.L. Valenzuela-Garcia, L.S. Quiroz-Castillo, P.J. Herrera-Franco, Adsorption and desorption of a gold-iodide complex onto cellulose acetate membrane coated with polyaniline or polypyrrole: a comparative study, J. Mater. Sci. 46 (2011) 7466–7474.
[50] M.L. Liu, Y.Y. Zhang, M.L. Wang, C.Y. Deng, Q.J. Xie, S.Z. Yao, Adsorption of bovine serum albumin and fibrinogen on hydrophilicity-controllable surfaces of polypyrrole doped with dodecyl benzene sulfonate – a combined piezoelectric quartz crystal impedance and electrochemical impedance study, Polymer 47 (2006) 3372–3381.
[51] J. Wang, B. Deng, H. Chen, X.R. Wang, J.Z. Zheng, Removal of aqueous Hg(II) by polyaniline: sorption characteristics and mechanisms, Environ. Sci. Technol. 43 (2009) 5223–5228.
[52] J.J. Li, Q. Zhang, J.T. Feng, W. Yan, Synthesis of PPy-modified TiO_2 composite in H_2SO_4 solution and its novel adsorption characteristics for organic dyes, Chem. Eng. J. 225 (2013) 766–775.